IEEE Photonics Journal
An IEEE Photonics Society Publication

Open Access

Experimental Evaluation of OFDM-Based Underwater Visible Light Communication System

Volume 10, Number 5, September 2018

Salah Hessien
Sezer Can Tokgöz, ***Student Member, IEEE***
Noha Anous
Ali Boyacı, ***Member, IEEE***
Mohamed Abdallah, ***Senior Member, IEEE***
Khalid A. Qaraqe, ***Senior Member, IEEE***

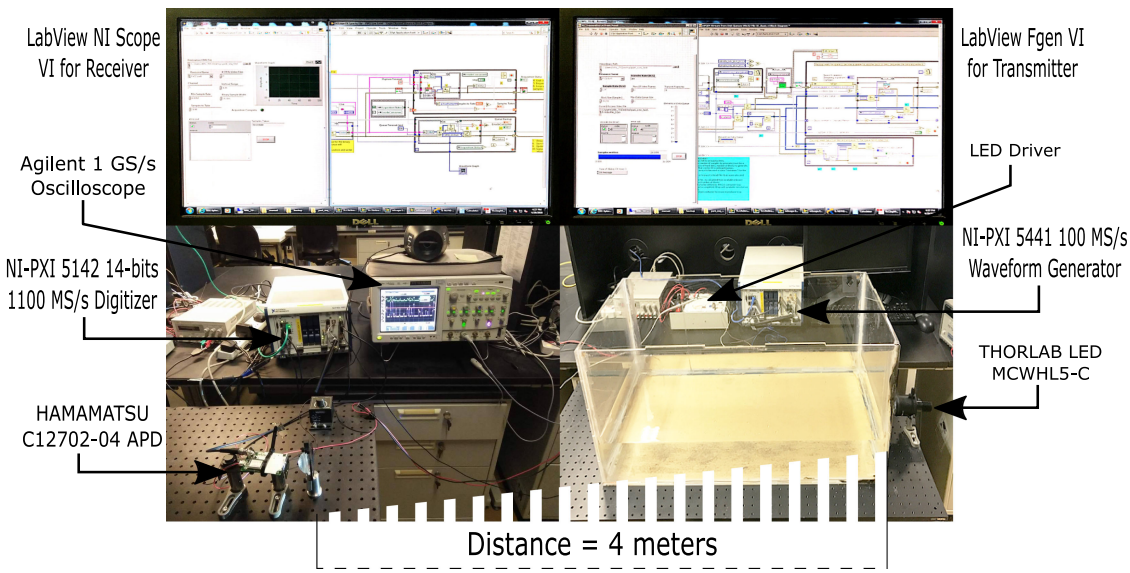

DOI: 10.1109/JPHOT.2018.2871958
1943-0655 © 2018 IEEE

Experimental Evaluation of OFDM-Based Underwater Visible Light Communication System

Salah Hessien,[1] **Sezer Can Tokgöz**,[1,2] ***Student Member, IEEE***,
Noha Anous,[1] **Ali Boyacı**,[1,3] ***Member, IEEE***,
Mohamed Abdallah,[4] ***Senior Member, IEEE***,
and Khalid A. Qaraqe,[1] ***Senior Member, IEEE***

[1]Department of Electrical and Computer Engineering, Texas A&M University at Qatar, Doha 23874, Qatar
[2]Department of Electrical and Electronics Engineering, Istanbul Commerce University, Istanbul 34453, Turkey
[3]Department of Computer Engineering, Istanbul Commerce University, Istanbul 34453, Turkey
[4]College of Science and Engineering, Hamad Bin Khalifa University, Qatar Foundation, Doha 34110, Qatar

DOI:10.1109/JPHOT.2018.2871958

Manuscript received July 30, 2018; revised August 25, 2018; accepted September 17, 2018. Date of publication September 28, 2018; date of current version October 10, 2018. This publication was made possible by the National Priorities Research Program (NPRP) award NPRP 9-077-2-036 from the Qatar National Research Fund (a member of The Qatar Foundation). Corresponding author: Sezer Can Tokgöz (e-mail: sezer_can.tokgoz@qatar.tamu.edu).

Abstract: High-speed, reliable, flexible, and cost-effective underwater wireless communication systems have a wide variety of use in scientific, civilian, and commercial domains. Visible light communication (VLC) seems to be a promising candidate in satisfying majority of the requirements listed above. From this perspective, VLC could easily be deployed in heterogeneous wireless networking scenarios with high quality of service. Therefore, in this paper, an adapted LTE frame structure is implemented for underwater VLC (UVLC) system. The performance of UVLC system employing asymmetrically clipped optical orthogonal frequency division multiplexing modulation technique is practically tested by taking channel estimation and synchronization into account. Also, the effects of varying orthogonal frequency division multiplexing parameters on the system's signal-to-noise ratio and the bit-error-rate (BER) performances are studied. The implementation is tested for quadrature phase shift keying and 16-quadrature amplitude modulation techniques supporting both 128- and 1024-points fast Fourier transform configurations, which correspond to data rates of 1.92 and 15.36 Mbps, respectively. Experimental results show that BER could be reduced down to a level on the order of 10^{-6}.

Index Terms: Optical wireless communication, underwater visible light communication, OFDM, 3GPP LTE Standard, performance evaluation, light emitting diode.

1. Introduction

Visible light communication (VLC) is currently introduced as a license-free communication system that is energy efficient, safe, secure, and that can be applied for underwater communications. Although underwater communications has started as a military field of interest in World War II, it

has not been used in scientific, civilian, and commercial applications until recently. However, the current acoustic technologies used for underwater applications cannot support the high demand of underwater systems due to its limited bandwidth, high latency, and transceiver complexity. Alternatively, underwater VLC (UVLC) has been recently considered as a promising cost-effective and reliable technology that can support high data rate. Additionally, VLC can be easily integrated with conventional underwater devices/infrastructures using their illumination systems by adding simple light emitting diodes (LEDs) and photodetectors (PDs) [1]–[3]. But it requires the line-of-sight (LOS) positioning, and it has limited range of communication compared to acoustic systems due to severe absorption, scattering, temperature fluctuations, and water turbidity [1], [4]. However, there are some possible solutions dealing with such phenomena to extend the communication range, e.g., MIMO transmission, relay-assisted transmission, and equalizer design/multiple symbol detection [5]–[9].

Different LED technologies offer white light illumination including phosphor-coated blue LEDs, red-green-blue (RGB) LEDs, gallium nitride (GaN) micro LEDs, and RGB laser diodes (LDs). Each technology supports a maximum data rate of 0.1, 5, 10, and 100 Gbps, respectively [10]. Despite supporting the lowest data rates, phosphor-coated LEDs are widely used due to their luminous stability with temperature variations, lower cost, and less hardware complexity [11].

One challenge in phosphor-coated LEDs is to fully utilize its limited bandwidth and combat intersymbol interference (ISI). A proposed solution is employing high-spectral efficiency modulation techniques such as orthogonal frequency division multiplexing (OFDM) that converts the high data rate serial signal into orthogonal sub-channels to overcome frequency selective fading resulting from the multipath effect [10], [11].

Most of the UVLC studies focus on increasing bandwidth and communication distance. These studies can be divided into two main categories employing LDs or LEDs at the transmitter side. For instance, an LD based UVLC link up to 2.2 Gbps over 12 m is demonstrated with a water tank of tap water in [12] using non-return-to-zero on-off keying modulation technique. The work in [13] develops OFDM based ultra-high-fidelity video transmission with 520 nm green LD over bi-directional underwater optical system supporting data rates of 15 Mbps for quadrature phase shift keying (QPSK), and 30 Mbps for both 16-quadrature amplitude modulation (16-QAM) and 64-QAM over 4.5 m. In [14], 8 m/9.6 Gbps underwater optical wireless communication (UOWC) system using a two-stage injection-locked 405 nm blue LD with 16-QAM is proposed, and a BER of 10^{-4} is achieved. However, LDs are not applicable for illumination and they can be considered harmful to living beings.

LED-based UOWC systems have shorter communication links and lower bandwidth compared to LDs, but they are more suitable to integrate into the existing devices/infrastructures. Multiple LEDs and multi-carrier modulation schemes are studied in the literature to increase the LED-based VLC performance. An underwater optical modem is implemented in [15] employing a 440 nm blue LED array of seven chips supporting 10 Mbps Manchester-coded signal over 10 m communication link. The work in [16] develops a long-distance UVLC system using on-off-keying, where the half-power angle of LED is narrowed to enhance the optical intensity as a transmitter, and a single photon avalanche diode (SPAD) are employed as a receiver. Simulation results show 10^{-6} of BER is achievable for 10 W power consumption with the data rate of 100 Mbps over 110 m. In [17] and [18], MIMO method is applied to UVLC systems using multiple LEDs, but less than 1 m communication links are established with poor performances and very low data rates. The authors in [19] and [20] introduce OFDM to the designed systems. In [19], DC biased optical-OFDM (DCO-OFDM) based VLC system is proposed with 10^{-4} of BER using 16-QAM. Coded-OFDM over short-range UVLC is considered in [20] supporting data rate of 1 Mbps up to 10^{-4} of BER.

Major themes of the existing studies are to achieve the highest data rate possible. Despite all of these valuable studies/contributions, a physical layer implementation of standard compliant OFDM system is missing. Therefore, in this study, 3GPP LTE rel. 8 Standard [21] is adapted and implemented for OFDM based UVLC system. The feasibility of UVLC employing asymmetrically clipped optical-OFDM (ACO-OFDM) modulation technique and widely used commercial white LEDs at nominal wavelength 440 nm is practically tested. The effects of varying OFDM parameters on the system's signal-to-noise ratio (SNR) and the BER performances are observed. The implementation

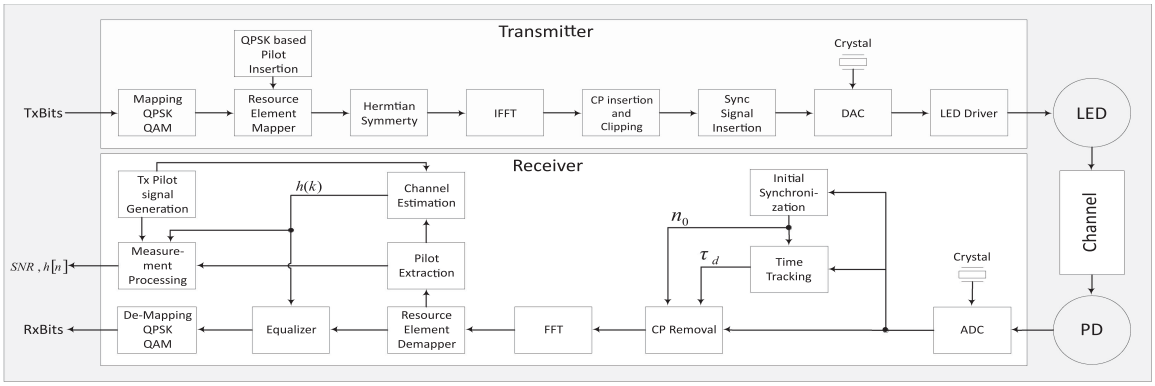

Fig. 1. VLC system-level architecture under study.

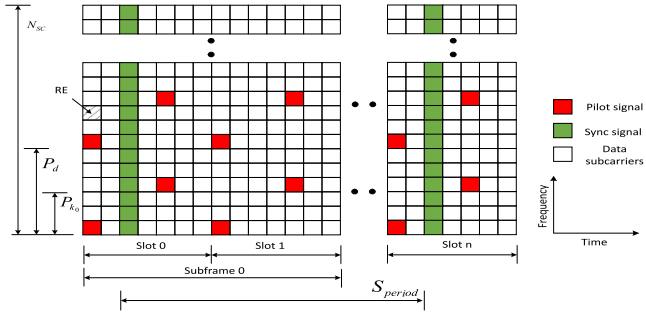

Fig. 2. VLC time-frequency lattice for OFDM transmission.

is tested for QPSK and 16-QAM modulation techniques supporting both 128- and 1024-points fast Fourier transform (FFT) configurations of 3GPP LTE rel. 8 Standard which correspond to data rates of 1.92 Mbps and 15.36 Mbps, respectively. Also, the practical implications of using timing synchronization and pilot-based practical channel estimation techniques are also discussed. In addition to this, free-space channel profile is compared with the underwater channel profile for different scenarios [22].

This paper is organized as follows. The detailed system model is presented in Section 2. In Section 3, experimental setup and organization are described. Experimental results are given and discussed in Section 4. Finally, Section 5 concludes the paper.

2. System Model

In this section, the system model is represented including VLC frame structure, signal model, initial synchronization and time tracking, channel estimation algorithm, and measurement processing. The architecture of the VLC system under study is illustrated in Figure 1.

2.1 VLC Frame Structure

LTE frequency division duplexing (FDD) frame structure [21] is adopted for the VLC system in this study. Each VLC frame consumes 10 ms and is divided into ten sub-frames, 1 ms each. An illustration of VLC time-frequency resource grid for normal cyclic prefix (CP) OFDM signal is shown in Figure 2. Each sub-frame has 14 symbols and further logically divided into two slots, each of 0.5 ms. A resource element (RE) is the smallest modulation unit which consists of one OFDM sub-carrier. In order to allow channel estimation at the receiver side, QPSK modulated pilot symbols are inserted into the OFDM time-frequency grid within the first and third last OFDM symbols of

TABLE 1
Physical Layer Parameters of the VLC System

Parameters	Values		Description
BW	1.4	10	Channel Bandwidth (MHz)
Δf	15		Sub-carrier Spacing (kHz)
f_s	1.92	15.36	Sampling Rate (MHz)
N_{RB}	6	50	Number of Resource Blocks
N_{SC}	72	600	Number of Occupied Subcarriers
N	128	1024	FFT Size
N_{sf}	1920	15360	Number of Samples per Subframe
CP	Normal		Cyclic Prefix Type
N_G	10/9	74/73	CP Size (first symbol/sixth following symbol)
P_d	6	12	Pilots Frequency Spacing
P_{k_0}	3	6	Pilots Frequency Offset
N_{sync}	72		Park's Sequence Length
S_{period}	20		Synchronization Pattern Periodicity (ms)

each slot with a frequency domain spacing of P_d sub-carriers. Moreover, there is a frequency domain shift of P_{k_0} sub-carrier between pilot symbols to allow channel estimation interpolation over multiple pilot symbols. An adapted Park's sequence [23] X_s of length N_{sync} is selected for VLC initial synchronization and time tacking. The synchronization pattern is transmitted with S_{period} periodicity in the resource grid.

Table 1 summarizes the main physical layer parameters supported by proposed VLC system model.

2.2 Signal Model

The input bits are mapped into complex symbols depending on the specified modulation technique. Then, QPSK pilot symbols are inserted into the VLC time-frequency grid using the *resource element mapper*. The OFDM signal is generated by applying inverse FFT (*IFFT*) as follows,

$$x(t) = \mathcal{IFFT}\left\{X(k)\right\} = \frac{1}{\sqrt{N}} \sum_{k=0}^{N-1} X(k) e^{\frac{j2\pi kt}{NT_s}} \tag{1}$$

where T_s is the ideal sampling period of digital-to-analog converter (DAC) at the transmitter. In ACO-OFDM, the modulated signal $X(k)$ is constrained to satisfy Hermitian symmetry to obtain a real-valued signal at the output of the IFFT block, which could directly modulate the intensity of the LED. Therefore, $X(k)$ is expressed as,

$$X(k) = \left[0,\ X_0,\ X_1,\ \ldots,\ X_{\frac{N}{2}-1},\ 0,\ X^*_{\frac{N}{2}-1},\ \ldots,\ X^*_1,\ X^*_0\right] \tag{2}$$

A CP is also added as a preamble to mitigate ISI,

$$x(n) = \begin{cases} x(N+n), & n = -N_G,\ -N_G+1,\ \ldots,\ N-1 \\ x(n), & n = 0,\ 1,\ \ldots,\ N-1 \end{cases} \tag{3}$$

where N_G denotes the number of CP depending on the time interval between the first and last channel paths. Then, the negative parts of the real-valued symbol are clipped as zero. Before DAC block, a synchronization signal is inserted for timing synchronization. Intensity modulated signal passes through the UVLC channel. The received continuous-time waveform is sampled at an interval of T_r instead of T_s due to the mismatch between the transmitter and receiver oscillators. The sampling frequency offset (SFO) can be defined as $\Delta f_s = \frac{1}{T_r} - \frac{1}{T_s}$ which can be written as

$T_r = \frac{T_s}{1+T_s\Delta f_s} = \frac{T_s}{1+\epsilon_s}$ where ϵ_s is the normalized SFO error that is usually defined in part-per-millions (ppm). Then, under the effect of SFO, the received baseband signal is obtained as,

$$Y(m) = \mathcal{FFT}\left\{y(n)\right\} = \frac{1}{\sqrt{N}}\sum_{n=0}^{N-1} y(n)e^{\frac{-j2\pi nm}{N}} \tag{4}$$

where,

$$y(n) = \frac{1}{\sqrt{N}}\sum_{k=0}^{N-1} X(k)H(k)e^{\frac{j2\pi knT_r}{NT_s}} \tag{5}$$

by substituting (5) into (4), $Y(m)$ yields,

$$Y(m) = \frac{1}{N}\sum_{n=0}^{N-1}\left[\sum_{k=0}^{N-1} X(k)H(k)e^{\frac{j2\pi knT_r}{NT_s}}\right]e^{\frac{-j2\pi nm}{N}} + W(k) \tag{6}$$

where $H(k)$ is the frequency response of the channel, and $W(k)$ is the sampled received noise term. In order to view the effect of SFO, it is processed further to yield the below representation,

$$Y(m) = \frac{1}{N}\sum_{k=0}^{N-1} X(k)H(k)\left[\sum_{n=0}^{N-1} e^{\frac{j2\pi n}{N}\left(\frac{kT_r}{T_s}-m\right)}\right] + W(k) \tag{7}$$

After substituting, rearranging, and using the notation of $\sum_{n=0}^{N-1} r^n = \frac{1-r^N}{1-r}$, $Y(m)$ is expressed as,

$$Y(m) = \frac{1}{N}\sum_{k=0}^{N-1} X(k)H(k)\left[\frac{\sin\left(\pi\left(m-\frac{kT_r}{T_s}\right)\right)}{\sin\left(\pi\left(m-\frac{kT_r}{T_s}\right)\frac{1}{N}\right)}e^{\frac{j2\pi}{N}\left(m-\frac{kT_r}{T_s}\right)(N-1)}\right] + W(k) \tag{8}$$

As seen here in (8), when satisfying $m = k$ to obtain relation between the frequency component at the T_x side and the corresponding one at the R_x side, it is obvious that the received symbol is scaled and phase rotated. Moreover, there is an inter carrier interferance (ICI) occurring from neighboring sub-carriers into the kth sub-carrier.

2.3 Initial Synchronization and Time Tracking

VLC synchronization signal is used to detect the OFDM symbol start point, n_0, by cross-correlating the incoming samples, $y(n)$, from PD front-end with the predefined synchronization sequence, X_s. The synchronization signal pattern is repeated every S_{period} in the time domain. The objective of the *correlation block* is to search for the symbol start value which maximizes the correlation between the received synchronization signal and the transmitted one. The correlation operation is represented as in [24],

$$R(k) = \sum_{n=k}^{k+N_{sync}-1} y(n)X_s\left(n+S_{period}\right) \tag{9}$$

Figure 3 shows time domain identified synchronization signals in the received signal under experimental study.

Once the initial synchronization is achieved, the *time tracking module* aims to track the integer samples τ_d that drifts due to the SFO. This time tracking does not account for the fractional timing as it is left to the channel estimation to handle it. The maximum time drift margin is set to 15 samples in the designed receiver. Moreover, the time tracking correlation result is averaged over multiple synchronization windows W_{sync} to form an accurate decision statistic R, where W_{sync} is multiple integers of S_{period}. The decision statistic is maximized to provide the estimated time drift τ_d. Then,

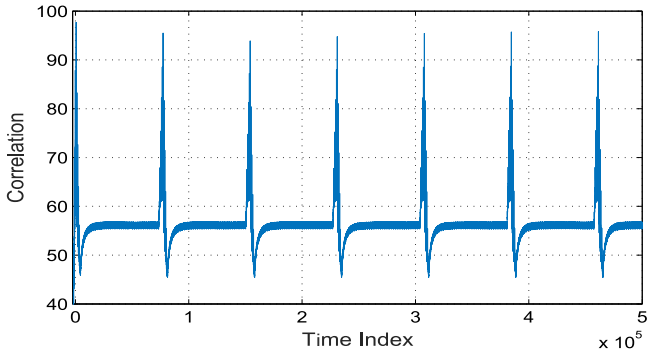

Fig. 3. Identified VLC frame synchronizations in time domain under experimental study.

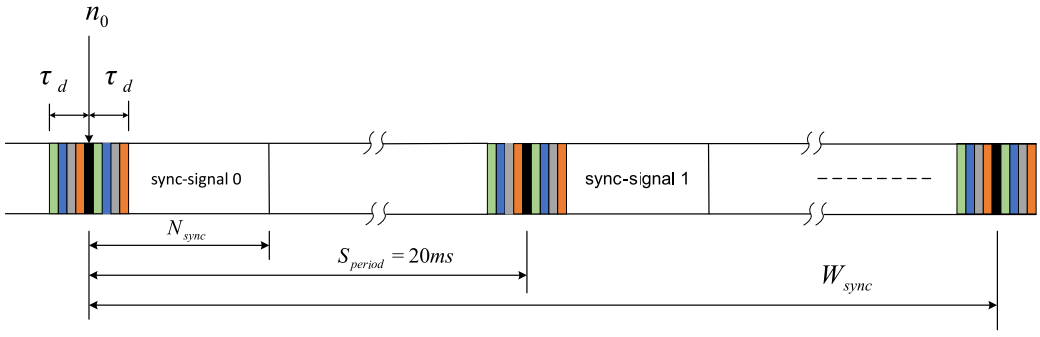

Fig. 4. VLC synchronization signal correlation for different symbol timing drifts.

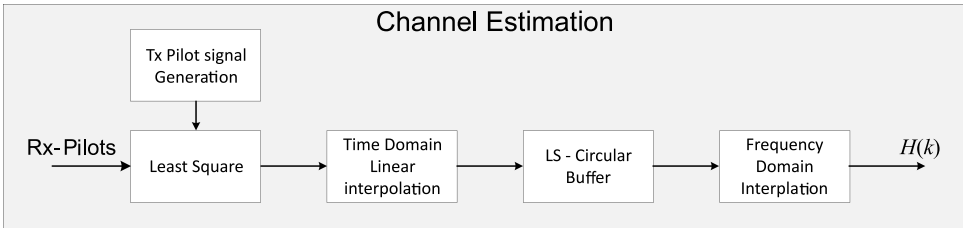

Fig. 5. VLC channel estimation block diagram.

the correlation operation can be represented as,

$$R(k) = \sum_{m=0}^{M-1} \left| \sum_{\substack{n=k \\ k \in [n_0-\tau_d, n_0+\tau_d]}}^{k+N_{sync}-1} y\left(n + mW_{sync}\right) X_s^*(n-k) \right| \tag{10}$$

The time tracking operation is simplified as shown in Figure 4. CP removal module is used to correct the estimated time drift τ_d by either inserting or dropping samples.

2.4 Channel Estimation

Once OFDM symbol boundaries are defined, CP is fully identified and removed. Therefore, the frequency domain calculation for each OFDM symbol is done using *FFT* operation. After *FFT*, the pilot symbols are extracted using *resource element demapper* for the channel estimation process. The 2D channel estimation is approximated to a 1D filtering in the frequency domain and linear interpolation in the time domain. The algorithm is applied to a single sub-frame as shown in Figure 5.

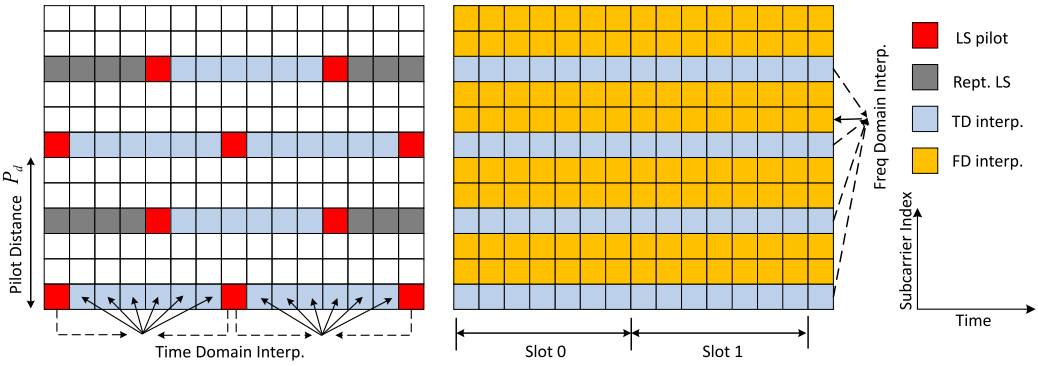

Fig. 6. VLC channel estimation process diagram.

The *least square (LS) block* performs channel estimation over the received pilot sub-carriers. These channel estimations are evaluated based on LS criteria as follow,

$$H(k_p) = \frac{Y(k_p)}{X(k_p)}, \qquad p = 0, 1, \ldots, \left\lfloor \frac{N_{SC}}{P_d} \right\rfloor \tag{11}$$

where $k_p = P_{k_0}(1 + pP_d)$ is the resource element index for channel estimation pilots, the variable P_{k_0} defines the pilot start position in the frequency domain for different OFDM symbols in VLC time-frequency resource grid. After LS pilot estimation, the *time-domain (TD) interpolation block* interpolates the pilot-based channel estimations between OFDM symbols to generate pilot-based channel estimations half-way $P_d/2$ between each symbol pair. *Frequency domain (FD) interpolation block* filters the available channel estimations over sub-carriers in order to obtain channel estimation of the entire OFDM symbols. For the kth sub-carrier in the processed OFDM symbol, the filtering operation generates channel estimation, $H(k)$, by a vector inner product of length N_{tap} over the N_{tap} closest available pilots channel estimation $H(k_{pj})$ as,

$$H(k) = \sum_{j=0}^{N_{tap}-1} H(k_{pj}).c[j], \qquad k = 0, 1, \ldots N_{SC} - 1 \tag{12}$$

where N_{tap} is the filter number of taps which equals 11 in the proposed design. The filter coefficients $c(j)$ are designed as a simple moving average filter (i.e., $c(j) = 1/N_{tap}$). Figure 6 illustrates the steps of the channel estimation process on VLC time-frequency grid. The channel estimations for the remaining sub-carriers (marked with gray color in Figure 6) are assumed to be constant due to the lack of pilots and it will be copied from the nearest available LS.

2.5 Measurement Processing

VLC measurement block is responsible for computing two indicators in order to maintain the closed loop transmission between the receiver PD and LED. Also, it used to monitor received signal power for one or more of the LED terminals in case of relay-assisted underwater system, and selecting the potential relay path based on the evaluated performance value of each relay paths. UVLC system includes the following measurements:

1) Channel impulse response (CIR) and it's corresponding maximum excess delay τ_m and average delay of the multipath μ_τ are obtained by transforming the estimated channel frequency response $H(k)$ to the time domain sequence, $h(n) = \mathcal{IFFT}\{H(k)\}$. Next, $h(n)$ is averaged over multiple OFDM symbols in order to reduce the noise power inside CIR. The estimated CIR provides an indication of the existing sampling offset drift between the transmitter and receiver that need to be corrected during the initial synchronization and time tracking to keep PD closed loop with LED. Figure 7 shows the absolute value of the estimated CIR versus time for 15.36 MHz bandwidth.

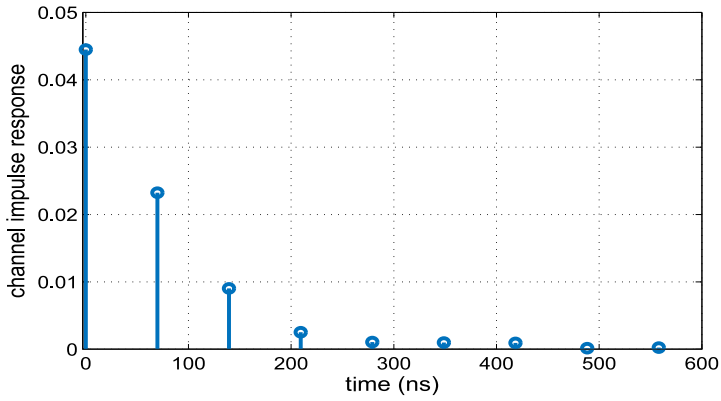

Fig. 7. UVLC channel impulse response for 15.36 MHz bandwidth. Maximum excess delay $\tau_m = 139$ ns, and average delay $\mu_\tau = 69$ ns.

2) The received SNR over the frequency spectrum is estimated using reference pilot signals by obtaining the following measurement metrics: (a) Reference signal received power, P_{RSRP}, defined in [25] which measures the power in the received pilot signals using,

$$P_{\text{RSRP}} = \frac{1}{M_{sf}} \sum_{n=0}^{M_{sf}-1} \sum_{k_p=0}^{\left\lfloor \frac{N_{SC}}{P_d} \right\rfloor - 1} H(k_p) H^*(k_p) \tag{13}$$

where M_{sf} is the number of sub-frames used for averaging measurement results over time, (b) Noise variance, σ_n, which measures the average noise power over the received pilot symbols using [25],

$$\sigma_n = \frac{1}{M_{sf}} \sum_{n=0}^{M_{sf}-1} \frac{1}{\lfloor N_{SC}/P_d \rfloor} \sum_{k_p=0}^{\left\lfloor \frac{N_{SC}}{P_d} \right\rfloor - 1} \left| Y(k_p) - H(k_p) X(k_p) \right|^2 \tag{14}$$

Then, the received SNR can be obtained based on (13) and (14) as follows,

$$\mathcal{SNR}_{dB} = 10 \log_{10} \left(\frac{P_{\text{RSRP}}}{\sigma_n} \right) \tag{15}$$

The received SNR metric is used for UVLC link performance evaluation for each conducted experiment in Section 3 below. Moreover, it can be used as a performance value for identifying a potential relay path in relay-assisted underwater system.

3. Experimental Setup

Measurements are taken in the Wireless Laboratory facilities at Texas A&M University at Qatar, Department of Electrical and Computer Engineering. All experiments are made under normal room illumination, and no optical filter is used to eliminate the ambient light. Figure 8 shows the experimental setup which consists of three main parts such as the transmitter, hybrid underwater/free-space channel, and receiver. In the transmitter part, NI PXI-5441 16-bit 100 MS/s arbitrary wave generator and THORLABS MCWHL5-C1 collimated white LED at nominal wavelength 440 nm are employed. A water tank of dimensions $(1 \times 0.4 \times 0.4)$ m^3 with 3 m free-space resembles the 4 m UVLC channel. The tank used in the experiment is made of acrylic and filled with fresh tap water to emulate the underwater horizontal channel. The attenuation coefficient of fresh tap water is estimated to be 0.071 m^{-1} [26]. Also, 4 m free-space link is studied and compared to the hybrid underwater/free-space link. In the receiver side, NI PXI-5142 14-bit 100 MSamples/s PXI digitizer and Hamamatsu C12702-04 avalanche photodiode (APD) modules are used. The employed APD

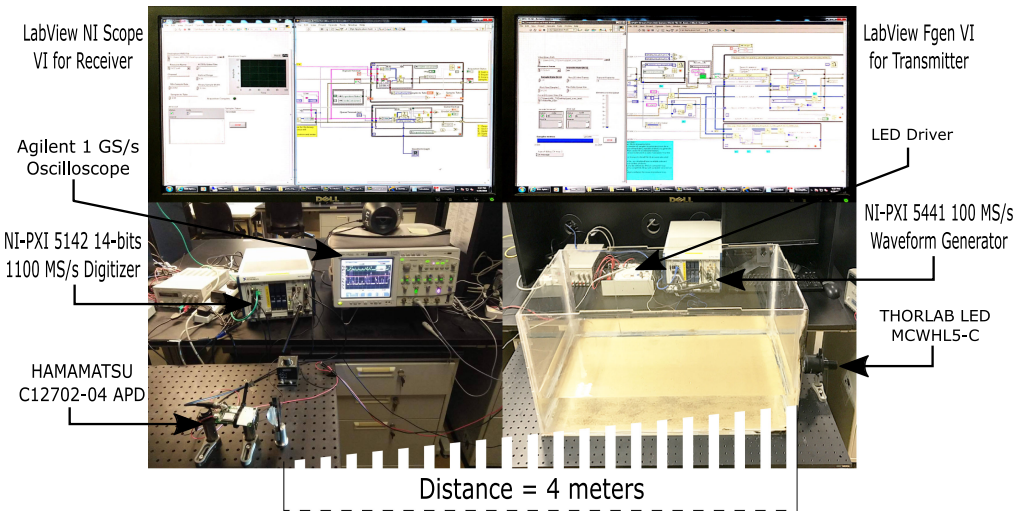

Fig. 8. Experimental setup under study.

possess an active area of 3 mm and a peak response at a wavelength λ of 800 nm. This APD has a 3 dB bandwidth of 4 kHz to 80 MHz, which is suitable to data rates employed in this work. A lens is placed before the APD for the sake of focusing the diverging light beam falling onto the APD. In addition to these devices, MSO8104A Infiniium 1 GHz bandwidth mixed signal oscilloscope is used testing and alignment of the transmitter and receiver pair for line-of-sight (LOS) positioning. The experiment consists of four essential parts including pre-processing, transmission, reception, and post-processing.

3.1 Pre-Processing

Transmitter model in Figure 1 is implemented using MATLAB software in which random bits are generated using a random number generator with a pre-defined seed. The generated data is coded with different modulation techniques such as QPSK or 16-QAM. Modulated complex data is then converted to parallel streams, and pre-generated pilot sequences are inserted for channel estimation. After IFFT operation, CP and synchronization signal are also inserted into the signal. The results are converted into a serial stream again and saved in a binary file for transmission.

3.2 Transmission

The generated data is transferred to the NI PXIe-1082 device, read from the hard drive and is sent to NI PXI-5441 DAC by using NI LabVIEW. The output is then sent to the designed LED driver to create intensity modulated signal which passes through communication channel with a data rate of 1.92 Mbps or 15.36 Mbps depending on the configuration.

3.3 Reception

The transferred intensity modulated signal is captured by Hamamatsu C12702-04 APD. The output of the APD is processed by NI PXI-5541 digitizer. Digital results are saved to the hard drive for post-processing.

3.4 Post-Processing

Receiver model in Figure 1 is also implemented using MATLAB software for processing the received data. Firstly, synchronization signal is identified, then the CP is removed, and the data is converted

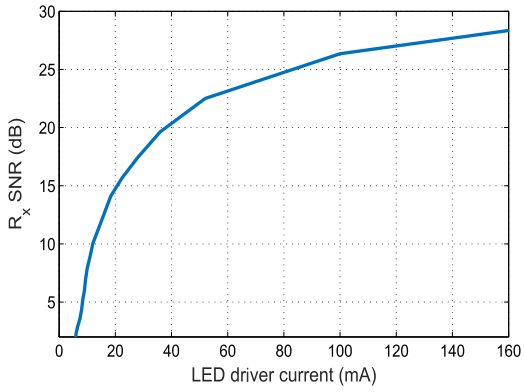

Fig. 9. SNR values of the experiment as a function of LED driver current.

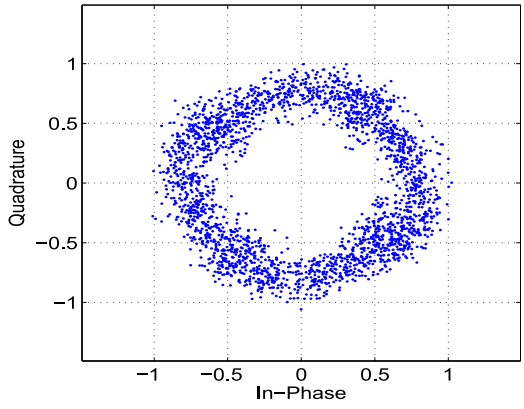

Fig. 10. R_x constellation with the effect of SFO.

to the parallel streams. After FFT operation, channel estimation and equalization is made. The resulting output is converted to serial stream again. Finally, the data is demodulated and decoded.

4. Results and Discussion

In this experiment, an UVLC system is built as previously illustrated. The system performance is tested for free-space and hybrid underwater/free-space channels. Also, the system performance is observed through SNR and BER behaviors under different physical layer parameters such as varying OFDM guard period and FFT sizes. The received SNR over the frequency spectrum is changed by adjusting the current limiter resistor of LED driver to control LED drawn current. Figure 9 shows the relation between the received SNR and LED forward current I_f. The SNR first increases linearly with the LED current then it tends to be saturated. The relationship is consistent with the nonlinear transfer characteristic of the LED current and the corresponding radiated optical power, P_{opt} [27].

Figure 10 depicts the effect of SFO on the received constellation diagram. As expected by equation 8, the amplitude and phase of the received baseband signal are distorted, which validates the above models. SFO is estimated and corrected using synchronization signal.

The free-space and hybrid channels are compared in terms of different FFT sizes and modulation techniques in Figure 11. The relationship between maximum excess delay, τ_m, and OFDM symbol duration determines the effect of the channel on the system performance. The received multipath components can destroy the sub-carrier orthogonality introducing ISI. In higher sampling rates, the proposed system is less tolerant to multipath because of the frequency selectivity of

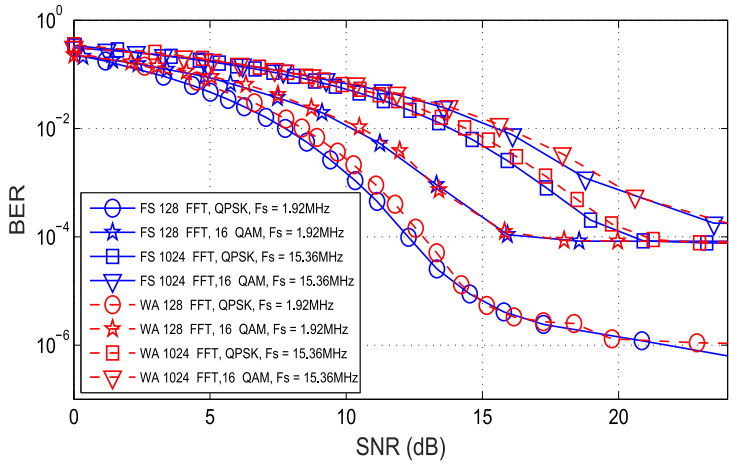

Fig. 11. Effects of the different sampling rates on the system's BER performance for free-space (FS) and water/acrylic (WA) channels using QPSK and 16-QAM modulations with enabled guard intervals.

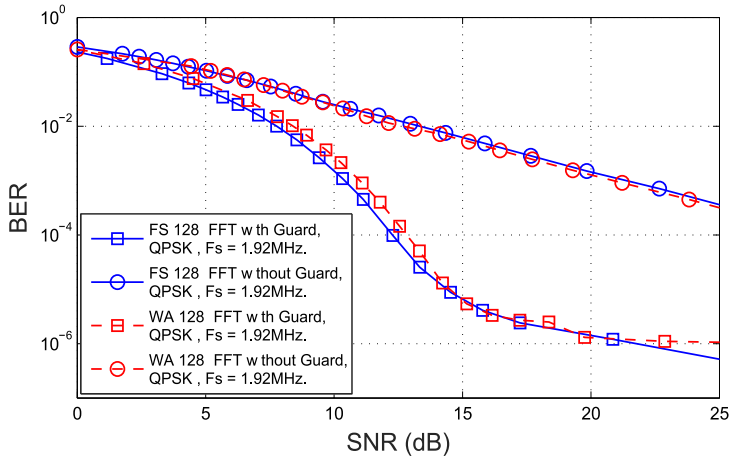

Fig. 12. Effects of the guard interval on the system's BER performance for free-space (FS) and water/acrylic (WA) channels using QPSK modulation.

the channel. Therefore, in higher sampling rates, advanced estimation and adaptive modulation techniques should be used to compensate this problem, however this will increase the complexity transmitter/receiver design.

In Figure 12, the effects of guard intervals in OFDM signal is shown for different channels using QPSK modulation. Usage of the guard intervals has an apparent effect on BER performance. Introducing guard intervals increase the system performance, however, decreasing number of active sub-carriers reduces the system throughput depending on OFDM configuration as given in Table 1.

Figure 13 shows the constellation maps for both QPSK and 16-QAM modulated signals over the 4 m hybrid channel with 1.92 MHz sampling rate. Results indicate that clear constellation diagrams can be obtained at 15 dB SNR up to 5×10^{-6} BER.

5. Conclusion and Future Work

In this paper, the 3GPP LTE physical layer standard is adapted and implemented for UVLC systems. The feasibility of UVLC employing ACO-OFDM modulation technique is practically tested for widely

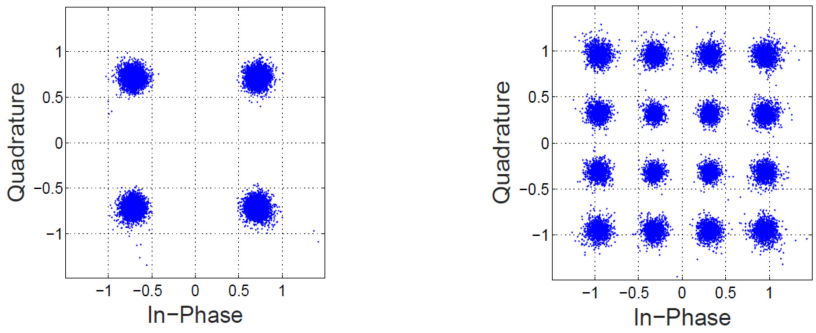

Fig. 13. Constellation maps of the QPSK and 16-QAM modulated R_x signals for 15 dB SNR with 1.92 MHz sampling rate, left to right respectively.

used commercial white LEDs and APDs. Also, the implementation is evaluated for QPSK and 16-QAM modulation techniques supporting both 128- and 1024-points FFT configurations of 3GPP LTE standard which correspond to data rates of 1.92 Mbps and 15.36 Mbps, respectively. The results indicate that high bandwidth UVLC system can be achieved with BER of 10^{-6} which is suitable for emerging bandwidth-hungry underwater applications such as image or video transmissions. The channel and noise statistics of the UVLC channel have been measured at higher sampling rates with comparing it to the free-space VLC channel. Moreover, the practical implications of using timing synchronization and pilot-based channel estimation techniques are also discussed in detail. The Park's sequence is used instead of primary (PSS)/secondary (SSS) LTE synchronization signals to achieve the VLC initial synchronization and time tacking. The synchronization signal periodicity is extended to 20 ms in our model to reduce the bandwidth overhead. In addition to this, free-space channel is compared to a hybrid underwater/free-space channel for different scenarios.

VLC is applicable to be used in various areas with a relatively simple transmitter/receiver design. However, its inherent shortcomings like direct LOS requirement and non-negative nature of light limits the system performance. To overcome these limitations, advanced processing techniques must be utilized, but these techniques increase the complexity of the transmitter/receiver design.

As a future work, the system will be tested under different conditions and scenarios. Higher-order modulations will be implemented with different data rates. In an attempt to improve system performance, advanced OFDM synchronization, pilot-based channel estimation, interference mitigation, and adaptive modulation techniques in the VLC system will be addressed.

Acknowledgment

The authors wish to thank the anonymous reviewers and the Associate Editor for their valuable suggestions.

References

[1] Z. Zeng, S. Fu, H. Zhang, Y. Dong, and J. Cheng, "A survey of underwater optical wireless communications," *IEEE Commun. Surveys Tut.*, vol. 19, no. 1, pp. 204–238, Jan.–Mar. 2017.
[2] M. Kashef, M. Ismail, M. Abdallah, K. A. Qaraqe, and E. Serpedin, "Energy efficient resource allocation for mixed RF/VLC heterogeneous wireless networks," *IEEE J. Select. Areas Commun.*, vol. 34, no. 4, pp. 883–893, Apr. 2016.
[3] N. Anous, M. Abdallah, M. Kashef, and K. Qaraqe, "A VLC-based system for optical SPR sensing facility," in *Proc. 2016 IEEE Wireless Commun. Netw. Conf.*, Apr. 2016, pp. 1–6.
[4] H. Kaushal and G. Kaddoum, "Underwater optical wireless communication," *IEEE Access*, vol. 4, pp. 1518–1547, 2016.
[5] M. V. Jamali, J. A. Salehi, and F. Akhoundi, "Performance studies of underwater wireless optical communication systems with spatial diversity: MIMO scheme," *IEEE Trans. Commun.*, vol. 65, no. 3, pp. 1176–1192, Mar. 2017.
[6] H. Zhang and Y. Dong, "Impulse response modeling for general underwater wireless optical MIMO links," *IEEE Commun. Mag.*, vol. 54, no. 2, pp. 56–61, Feb. 2016.
[7] M. V. Jamali, A. Chizari, and J. A. Salehi, "Performance analysis of multi-hop underwater wireless optical communication systems," *IEEE Photon. Technol. Lett.*, vol. 29, no. 5, pp. 462–465, Mar. 2017.

[8] A. Celik, N. Saeed, T. Y. Al-Naffouri, and M. Alouini, "Modeling and performance analysis of multihop underwater optical wireless sensor networks," in *Proc. 2018 IEEE Wireless Commun. Netw. Conf.*, Apr. 2018, pp. 1–6.
[9] M. V. Jamali, P. Nabavi, and J. A. Salehi, "MIMO underwater visible light communications: Comprehensive channel study, performance analysis, and multiple-symbol detection," *IEEE Trans. Veh. Technol.*, vol. 67, no. 9, pp. 8223–8237, Sep. 2018.
[10] P. H. Pathak, X. Feng, P. Hu, and P. Mohapatra, "Visible light communication, networking, and sensing: A survey, potential and challenges," *IEEE Commun. Surveys Tut.*, vol. 17, no. 4, pp. 2047–2077, Oct.–Dec. 2015.
[11] C. Hongda *et al.*, "Advances and prospects in visible light communications," *J. Semiconductors*, vol. 37, no. 1, 2016, Art. no. 011001.
[12] C. Shen *et al.*, "Going beyond 10-meter, Gbit/s underwater optical wireless communication links based on visible lasers," in *Proc. 2017 Opto-Electron. Commun. Conf. Photon. Global Conf.*, Jul. 2017, pp. 1–3.
[13] A. Alhalafi and B. Shihada, "UHD video transmission over bi-directional underwater wireless optical communication," *IEEE Photon. J.*, vol. 10, no. 2, Apr. 2018, Art. no. 7902914.
[14] H. H. Lu *et al.*, "An 8 m/9.6 Gbps underwater wireless optical communication system," *IEEE Photon. J.*, vol. 8, no. 5, Oct. 2016, Art. no. 7906107.
[15] G. Cossu, A. Sturniolo, A. Messa, D. Scaradozzi, and E. Ciaramella, "Full-fledged 10Base-T ethernet underwater optical wireless communication system," *IEEE J. Select. Areas. Commun.*, vol. 36, no. 1, pp. 194–202, Jan. 2018.
[16] C. Wang, H. Y. Yu, and Y. J. Zhu, "A long distance underwater visible light communication system with single photon avalanche diode," *IEEE Photon. J.*, vol. 8, no. 5, Oct. 2016, Art. no. 7906311.
[17] M. S. M. Akram, L. G. D. Aravinda, M. K. P. D. Munaweera, G. M. R. I. Godaliyadda, and M. P. B. Ekanayake, "Camera based visible light communication system for underwater applications," in *Proc. 2017 IEEE Int. Conf. Ind. Inf. Syst.*, Dec. 2017, pp. 1–6.
[18] P. D. Munaweera, M. Akram, D. Aravinda, R. I. Godaliyadda, and P. B. Ekanayake, "Design and analysis of an under water visible light MIMO communication system with a camera receiver," in *Proc. 2017 17th Int. Conf. Advances ICT Emerging Regions.*, Sep. 2017, pp. 1–7.
[19] Y. D. Zang, J. Zhang, and L. H. Si-Ma, "Anscombe root DCO-OFDM for SPAD-based visible light communication," *IEEE Photon. J.*, vol. 10, no. 2, Apr. 2018, Art. no. 7902509.
[20] J. Alkhasraji and C. Tsimenidis, "Coded OFDM over short range underwater optical wireless channels using LED," in *Proc. OCEANS 2017 - Aberdeen*, Jun. 2017, pp. 1–7.
[21] *LTE; Evolved Universal Terrestrial Radio Access (E-UTRA); Physical Channels and Modulation (3GPP TS 36.211 Version 10.0.0 Release 10)*, ETSI TS 136 211 V10.0.0 (2011-01), 2011.
[22] J. A. Simpson, B. L. Hughes, and J. F. Muth, "Smart transmitters and receivers for underwater free-space optical communication," *IEEE J. Select. Areas Commun.*, vol. 30, no. 5, pp. 964–974, Jun. 2012.
[23] M. F. G. Medina, O. González, S. Rodríguez, and I. R. Martín, "Timing synchronization for OFDM-based visible light communication system," in *Proc. 2016 Wireless Telecommun. Symp.*, Apr. 2016, pp. 1–4.
[24] S. Tian, K. Panta, H. A. Suraweera, B. J. C. S. J. C. Schmidt, S. McLaughlin, and J. Armstrong, "A novel timing synchronization method for ACO-OFDM-based optical wireless communications," *IEEE Trans. Wireless Commun.*, vol. 7, no. 12, pp. 4958–4967, Dec. 2008.
[25] *LTE; Evolved Universal Terrestrial Radio Access (E-UTRA); Physical layer; Measurements (3GPP TS 36.214 Version 10.1.0 Release 10)*, ETSI TS 136 211 V10.0.0 (2011-01), 2011.
[26] J. W. Giles and I. N. Bankman, "Underwater optical communications systems. Part 2: Basic design considerations," in *Proc. IEEE Military Commun. Conf.*, vol. 3, Oct. 2005, pp. 1700–1705.
[27] S. Dimitrov and H. Haas, "Information rate of OFDM-based optical wireless communication systems with nonlinear distortion," *J. Lightw. Technol.*, vol. 31, no. 6, pp. 918–929, Mar. 2013.